

1 **Insights into Lightning K-Leader Initiation and**
2 **Development from Three Dimensional Broadband**
3 **Interferometric Observations**

4 **Daniel P. Jensen**^{1,2}, **Xuan-Min Shao**¹, and **Richard G. Sonnenfeld**²

5 ¹Los Alamos National Laboratory, Los Alamos, NM, USA

6 ²Langmuir Laboratory, New Mexico Institute of Mining and Technology, Socorro, NM, USA

7 **Key Points:**

- 8 • K-leader propagation often exhibits an initial acceleration followed by a gradual
9 deceleration
10 • K-leaders often sharply decelerate and then sharply re-accelerate as they approach
11 and pass branch junctions in the flash structure
12 • A bidirectionally extending region of “twinkling” VHF sources leads to the ini-
13 tiation of the next K-leader

Corresponding author: Daniel Jensen, djensen@alumni.nmt.edu

14 Abstract

15 We report detailed observations of K-leaders and the activity between them with
 16 the three-dimensional Broadband Interferometric Mapping and Polarization system (BIMAP-
 17 3D) at Los Alamos National Laboratory. It is found that K-leaders have a general prop-
 18 agation trend of initial acceleration and then gradual deceleration, and the correspond-
 19 ing very high frequency (VHF) radiation power is exponentially correlated with the leader
 20 speed. Based on the 3D development and simultaneous electric field change measurement,
 21 some simple K-leaders can be modeled with time-evolving point charges at the propa-
 22 gating leader tip and at the stationary origin. We found that the charge magnitude in-
 23 creases during the initial acceleration stage and stays relatively constant for the rest of
 24 the development. K-leaders are observed to interact with other branches; the branches
 25 affect the leader’s propagation speed, and may affect the charge transfer. After the oc-
 26 currence of a K-leader, VHF emissions are quenched for several milliseconds. VHF sources
 27 then reappear in an impulsive and scattered manner as “twinkling”, and these sources
 28 are found not uniquely on the so-called needles, but also on the main channel. These twin-
 29 kling sources start near the apparent positive leader tip, and extend back towards the
 30 direction of the flash origin at about 10^5 m/s, while the apparent positive tip continues
 31 to extend forward at about 10^4 m/s. The twinkling extending towards the direction of
 32 flash origin appears to initiate the following K-leader, although it may be interrupted
 33 by a K-leader along a different branch, or simply die out without more K-leader activ-
 34 ity.

35 Plain Language Summary

36 A K-leader is a discharge process that occurs at the later stage of a lightning flash.
 37 It retraces the path established by earlier discharges and propagates at a high speed of
 38 10^6 - 10^7 m/s. Recently we developed a new system called BIMAP-3D that can map light-
 39 ning radio sources in 3D at a spatial resolution of 10 meters and at a time resolution of
 40 a fraction of a microsecond. We found that K-leaders commonly speed up from 10^6 to
 41 10^7 m/s at the initial stage and then gradually slow down to a stop at their later stage,
 42 with associated radio power positively correlated with the traveling speed. Other branches
 43 in the lightning flash are found to affect the K-leader speed as it approaches and passes
 44 the branch junctions due to charge redistribution caused by the earlier processes. Af-
 45 ter the occurrence of a K-leader radio emissions are shut off for a few milliseconds due
 46 to the increased conductivity of the leader. After that, scattered radio sources reappear
 47 in an expanding region, both extending the branch and expanding back towards the start-
 48 ing point of the lightning. These apparent twinkling radio sources lead to the start of
 49 the next K-leader.

50 1 Introduction

51 A K-leader is a lightning discharge process that retraces previously ionized chan-
 52 nels in a lightning flash, at speeds on the order of 10^7 m/s (Schonland et al., 1935; Loeb,
 53 1966; Jordan et al., 1992; Shao et al., 1995; Shao & Krehbiel, 1996; Stock et al., 2014).
 54 K-leaders begin on a channel in the positive breakdown region (typically with net nega-
 55 tive cloud charge density) and propagate in the direction of the negative breakdown re-
 56 gion (Shao et al., 1995; Stock et al., 2014; Jensen et al., 2021). They are occasionally ob-
 57 served turning “backwards” and propagating back down a different branch in the pos-
 58 itive breakdown direction (Stock et al., 2014; Shao et al., 2018, 2023). Recent high speed
 59 video observations for occasional out-of-cloud K-leader processes showed that K-leaders
 60 start near but not at the tips of the positive breakdown channels (Mazur, 2016; Ding et
 61 al., 2022). Very high frequency (VHF) radio observations show a similar initiation lo-
 62 cation (Hare et al., 2021; Jensen et al., 2021). K-leaders have been observed to commonly
 63 slow down as they propagate (Jordan et al., 1992; Stock et al., 2014; Jensen et al., 2021;

64 Hare et al., 2023), but sometimes to speed up for some fraction of their duration (Stock
 65 et al., 2014; Jensen et al., 2021; Hare et al., 2023). The mechanisms behind the changes
 66 of speed are not well understood, although Shao and Krehbiel (1996) reported that a K-
 67 leader which had a burst of activity near its starting point apparently renewed and in-
 68 tensified the breakdown activity at the negative end.

69 K-leaders are associated with an electric field change called a K-change (Kitagawa,
 70 1957). Winn et al. (2011) compared New Mexico Tech’s Lightning Mapping Array (LMA)
 71 observations with a balloon-borne electric field change measurement, and suggested that
 72 the field change is related to a relatively higher charge concentration at the propagat-
 73 ing leader tip. In this study the field change will be examined against the 3D K-leader
 74 development to better understand the charge distribution along the channel while the
 75 leader is propagating forward.

76 The process of K-leader initiation is even less well understood than the details of
 77 K-leader development and dynamics. K-leaders are observed to start in the positive break-
 78 down region, but unlike K-leaders themselves positive leaders are quiet at VHF and dif-
 79 ficult to map (Shao et al., 1999; Edens et al., 2012; Pu et al., 2021; Stock et al., 2023).
 80 VHF observations by Hare et al. (2019;2021) in this region have been attributed primar-
 81 ily to other processes such as needles around the channel rather than to the actual posi-
 82 tive leader tips. High speed video observations have provided insight into K-leader ini-
 83 tiation and development when it occurs outside of the cloud. All of these optical obser-
 84 vations show evidence of channel cutoff prior to K-leader initiation. That is, at the time
 85 when the K-leader becomes visible the connecting channel structure is optically dark,
 86 suggesting the channel is relatively cold and low in conductivity (Kong et al., 2008; Saba
 87 et al., 2008; Warner et al., 2012; Saraiva et al., 2014; Mazur, 2016; Wang et al., 2019;
 88 Huang et al., 2021; Jiang et al., 2022; Ding et al., 2022).

89 As noted by Jensen et al. (2021), there is a disagreement within the lightning com-
 90 munity about the proper terminology for the K-leader phenomenon. In Kitagawa (1957)
 91 where the term K-change was coined, the step-like field changes were attributed to pro-
 92 cesses similar to both recoil streamers and dart leaders. The leader associated with a K-
 93 change was later called a K streamer/leader (Shao et al., 1995; Stock et al., 2014). All
 94 three terms (dart leader, K-leader, recoil streamer/leader) and minor variations on them
 95 continue to be used today in the community (Winn et al., 2011; Stock et al., 2014; Akita
 96 et al., 2010; Hare et al., 2021) despite their generally recognized equivalence (Kitagawa,
 97 1957; Shao et al., 1995; Mazur, 2002; Stock et al., 2014; Mazur, 2016). A more complete
 98 discussion of the terminology and its history can be found in Rakov and Uman (2003)
 99 sections 4.10 and 9.5, Zhu et al. (2014), and Stolzenburg et al. (2015) section 6. In this
 100 paper we will exclusively use the term “K-leader” to refer to this phenomenon.

101 **2 The BIMAP-3D System**

102 We have recently introduced the Broadband Interferometric Mapping And Polariza-
 103 tion in 3D (BIMAP-3D) system at Los Alamos National Laboratory (LANL). BIMAP-
 104 3D consists of two stations separated by 11.5 km. Each station consists of four dual-polarization
 105 VHF antennas (20-80 MHz), which are combined to provide 2D source location and po-
 106 larization measurements. Results from the two stations are combined to give 3D loca-
 107 tion and polarization measurements. In this paper we will focus on the 3D location re-
 108 sults. In a favorable scenario when a lightning flash occurs at high altitude between the
 109 two stations K-leader channels can be mapped with a resolution of 10 m or better in the
 110 three coordinate directions (easting, northing, and altitude) (Shao et al., 2023). Each
 111 BIMAP-3D station also has a fast electric field change sensor, or fast antenna.

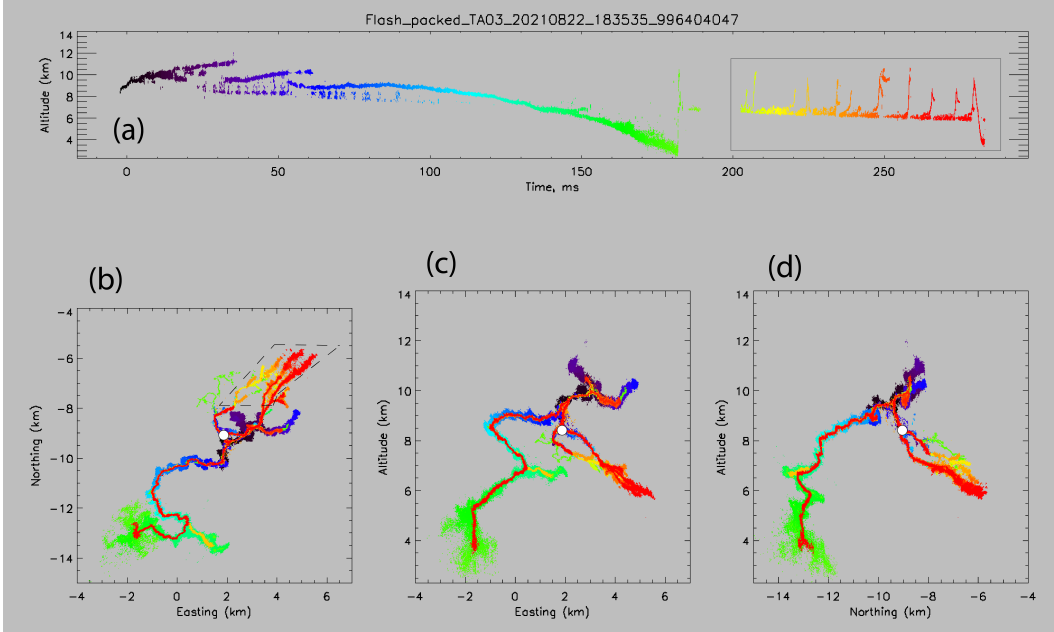


Figure 1. Overview of the presented flash, showing altitude (relative to sea level) vs time (a), northing vs easting (b), altitude vs easting (c), and altitude vs northing (d). The origin (zero) of the Easting/Northing coordinate system is defined as the position of the center antenna of the BIMAP1 station, while a white dot marks the flash origin point in panels b, c, and d. The K-leaders in the later part of the flash are boxed in panel a, and a region in panel b is marked with a dashed outline for closer inspection later in Section 6.

112

3 Flash Overview

113

114

115

116

117

118

119

120

121

122

123

124

125

126

The K-leaders presented in this paper occurred in a hybrid intra-cloud/cloud-to-ground (IC/CG) bolt-from-the-blue flash, and the flash's overall structure and development were reported earlier by Shao et al. (2023), as shown in Figure 1. Animation 1 in the supplementary material also provides an overview of the full flash development (Jensen et al., 2023). The flash begins as a typical IC, with the negative stepped leader growing upward. After about 20 ms scattered sources descend to around 8 km altitude (Figure 1a). Beginning at 50 ms, one of the negative leader branches grows from the origin to the southwest and eventually reaches the ground at about 180 ms, at a horizontal distance of 5.5 km from the flash origin. As the return stroke travels back up, it produces VHF sources at the tips of many earlier channels and branches, indicating that it attempts to neutralize previously deposited charge along these channels and branches. In addition, some new, fast-propagating, and positive breakdown branches were produced by the return strokes, e.g., the lime green branches in the region of 1 and 2 km easting and -6.5 and -8 km northing in Figure 1, similar to that reported in Shao et al. (1995).

127

128

129

130

131

132

133

134

The data gap between 190 ms and 205 ms is due to a lack of trigger in our instrumentation, suggesting any activity during this period was relatively quiet in VHF. After 200 ms nearly continuous activity extends the positive discharge region to the northeast while descending from 7.5 km to 6.5 km altitude. This gradual descent is periodically interrupted by 14 K-leaders which each rapidly retrace part of the existing channel structure. Most of the observed K-leaders occurred high above the ground in the cloud as normal intra-cloud K-leaders. The last K-leader in the data record propagated near to the ground along the initial leader channel but stopped at 2 km above the ground.

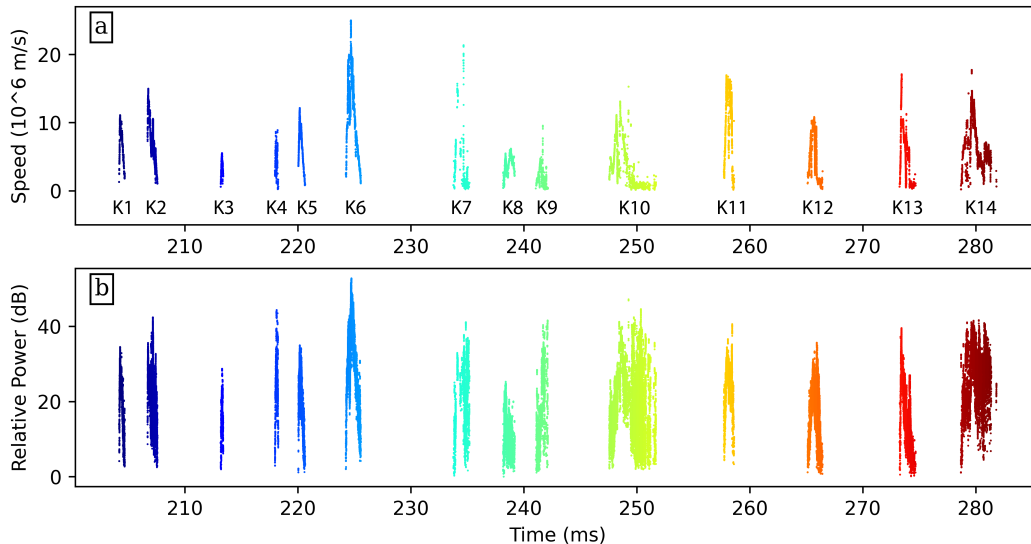


Figure 2. Plot of speed vs time (a) and VHF power vs time (b) for all the K-leaders from the analyzed flash. The K-leaders are labeled K1 through K14.

135 In this paper, we will investigate the K-leader and the inter-K-leader activities, marked
 136 with a box in Figure 1a. Animation 2 in the supplementary materials provides a clear
 137 view of the 3D development in this later portion of the flash (Jensen et al., 2023).

138 4 K-leader VHF Power and Propagation Speed

139 4.1 Overview of All K-leaders

140 Since we have not thoroughly calibrated our VHF antennas and the specific BIMAP
 141 receivers, we will not present VHF power in an absolute scale in this study. Instead, a
 142 relative measure of signal to noise ratio (SNR) will be used (Shao et al., 2020). In this
 143 case the “noise” level is determined by the lowest received power level among all the an-
 144 alyzed K leaders. SNR for each located source is referenced to this noise level, and is ad-
 145 justed by the distance from the source to the antennas. Since the results presented only
 146 concern trends of increasing and decreasing VHF power the lack of absolute calibration
 147 should not affect the validity of our conclusions.

148 To estimate K-leader propagation speed, a linear fit of the source position vs. time
 149 was taken in the three coordinate directions (x, y, z) respectively, giving a velocity vec-
 150 tor (V_x, V_y, V_z). The leader propagation speed is computed from the corresponding ve-
 151 locity vector. The linear fits were calculated in time windows of $\pm 15 \mu s$ centered on each
 152 source. In order to exclude errors in the velocity calculation caused by sources from mul-
 153 tiple simultaneous branches, we restricted sources to be within 500 m of each centered
 154 source. Under conservative estimates, the one sigma uncertainty in the speed calcula-
 155 tions is 10^5 m/s, at least an order of magnitude lower than all of the measured K-leader
 156 speeds, and is sufficiently low for this study. Appendix A provides full detail on how the
 157 speed uncertainty was calculated.

158 Figure 2a shows an overview of the speed and power vs time for all the K-leaders,
 159 and labels them K1 through K14. The path of each K-leader is shown in Animation 2
 160 in the supplementary materials (Jensen et al., 2023). As illustrated in Figure 2a, the K-
 161 leaders typically start and end at a lower speed, reaching a higher speed somewhere in

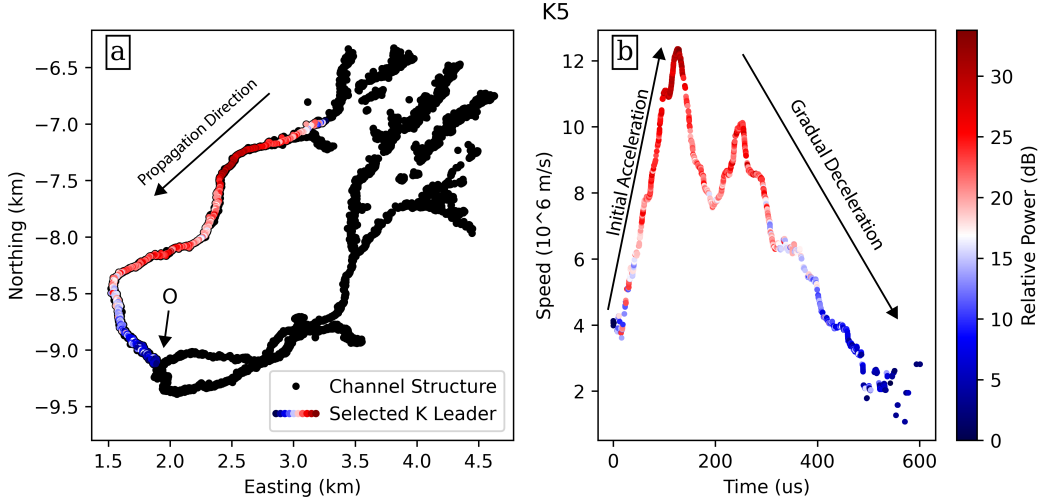


Figure 3. Plot of the path of the fifth K-leader (K5) with the background channel structure in Northing vs Easting (a), and the speed of K5 vs time (b). The K-leader sources in both panels are colored by relative VHF power. The flash origin is marked O, along with an arrow for the general propagation direction from the outer branches towards the origin. The first order trends of initial acceleration and gradual deceleration are also marked in panel b. The background channel structure in this figure is a zoomed in view of the full channel structure shown later in Figure 5.

162 the middle of their propagation, sometimes with significant variations throughout. A similar
 163 speed trend was reported by Jensen et al. (2021), although two of the leaders in that
 164 study apparently started near their maximum speed. The K-leaders analyzed by Hare
 165 et al. (2023) also generally follow these speed trends, although it is clear that individual
 166 K-leaders may deviate from the trends for part or all of their development.

167 Figure 2b shows relative VHF power vs time for these K-leaders. The same general
 168 trend as that of the propagation speed is observed. They commonly start and end
 169 with lower power levels and reach a higher power level in the middle of their develop-
 170 ment, apparently correlated with the speed of K-leader propagation. In a few cases the
 171 VHF power stayed high while the propagation speed has dropped down toward the end
 172 of the propagation, as seen for K10 and K14. These cases apparently correspond to a
 173 transition from a normal K-leader propagation to a more step-like propagation mode.
 174 This seems to be fairly common at the end of a K-leader's development, K7, K12, and
 175 K13 show similar behavior for their last 500 μ s or so with an average propagation speed
 176 of around 1×10^6 m/s. We infer the occurrence of stepping at the final stage of the K-
 177 leaders because of the observed large variations of VHF power and oscillations in the ap-
 178 parent propagation speed around a relatively constant and slower average speed. These
 179 features are similar to that of negative stepped leaders. The speed is also in agreement
 180 with the average dart-stepped leader speed of $(1 - 2) \times 10^6$ m/s reported in Table 1.1
 181 of Rakov and Uman (2003). We could not map any discrete structures associated with
 182 the individual steps due to the spatial and temporal resolutions of our current observa-
 183 tions. This apparent stepping propagation is marked in the supplementary figures (Jensen
 184 et al., 2023).

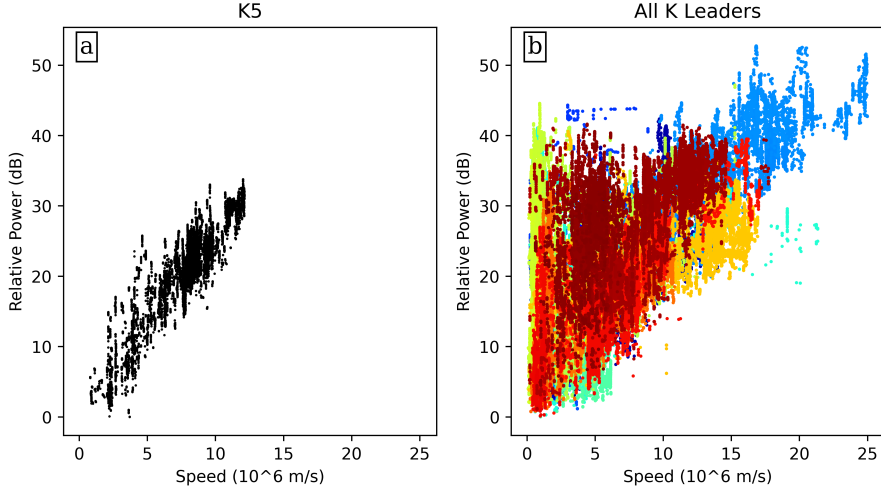


Figure 4. Plot of relative power vs speed for K5 (a), and for all K-leaders, colored by time (b).

185

4.2 Detailed Analysis of a Well Defined K-leader

186

187

188

189

190

191

192

193

194

195

196

197

198

199

We now examine the fifth K-leader (K5 in Figure 2) for detailed analysis. K5 propagates along a single branch and has a relatively simple speed behavior. Figure 3a shows the path of K5, extending about 3 km, with points colored by VHF power. In this plot the black dots show the background channel structure for this part of the flash. Figure 3b shows the speed vs. time of K5, again colored by VHF power. This simple K-leader clearly shows a strong initial acceleration from 4×10^6 m/s to its maximum speed of 12×10^6 m/s in the first $150 \mu\text{s}$. It then gradually decelerates to 2×10^6 m/s over the remaining $450 \mu\text{s}$, until the K-leader sources cease altogether. During the deceleration there is a temporary re-acceleration from $200 \mu\text{s}$ to $250 \mu\text{s}$. Speed variations like this are common and in some cases may overwhelm the typical acceleration or deceleration of the K-leader. Since the general dynamics of K-leaders are still not well understood we will focus on first order trends and leave other variations to future investigations. In general the way the speed of this K-leader changes over time is similar to those reported by Jensen et al. (2021) and Hare et al. (2023).

200

201

202

203

Figure 3b shows a strong correlation between the leader's speed and power, with the source power starting low, increasing to near its maximum at $150 \mu\text{s}$, and then dropping back down to the lowest power level toward the end of the K-leader. The relative power level for this K-leader changed from 0 to about 30 dB across its development.

204

205

206

207

208

209

210

211

212

213

214

Figure 4a shows the relative VHF power vs propagation speed for K5. The apparent linear relation between the propagation speed and the logarithmic power indicates an exponential relationship between the two parameters. These results are similar to those recently reported by Hare et al. (2023). Figure 4b is similar to Figure 4a but for all K-leaders in the flash (Figure 2). At low speed there seems to be a wide range of VHF source powers. However, much of this apparent scatter is due to the transition from smoother K-leader propagation to a more step-like propagation as noted for K10, K14, and several others. The correlation between VHF power and speed is still readily apparent at higher speeds for all 14 K-leaders. Apparently in the step-like propagation mode K-leaders can emit significantly higher VHF power than a more smoothly propagating K-leader at the same speed.

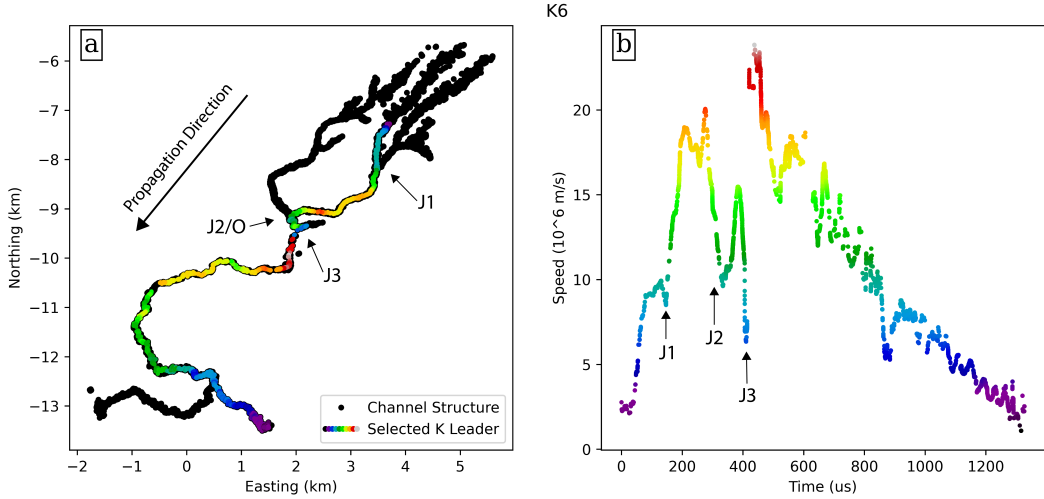


Figure 5. A plot of the path of the 6th K-leader (K6) relative to the overall branching structure in Easting vs Northing (a), and the speed of K6 vs time (b), with the K-leader points colored by speed. The junctions J1, J2, and J3, are marked in both panels. J2 is also at the flash origin, marked O. The general propagation direction is indicated with an arrow, K6 begins in the north and ends in the south end of the plot. This figure shows the full background channel structure for the flash, Figure 3 showed only the portion north of -9.5 km northing.

215

4.3 Effect of Branch Junctions on K-leader Speed

216

217

218

219

220

221

222

223

224

In the previous example we examined a K-leader propagating along a single branch. Figure 5 on the other hand shows the 6th K-leader (K6, Figure 2), which passes two branch junctions, or intersections. We now examine whether branch junctions affect the K-leader propagation speed. The black dots in Figure 5a now show the full background channel structure for the flash, whereas in Figure 3 only the northern portion of the channel structure was shown. The upper branch (extending from J3, Figure 5a) has been truncated to avoid the false appearance of junctions. This truncated branch is at higher altitude than the other branches but overlays them in easting and northing (Figures 1c and 1d). The K-leader path in Figure 5a and the points in Figure 5b are colored by speed.

225

226

227

228

229

230

231

232

233

234

K6 starts with a rapid initial acceleration from 1.5×10^6 m/s up to 9×10^6 m/s, and then reaches a speed plateau around $100 \mu\text{s}$. This occurs as the K-leader approaches the first junction (J1). After passing J1 the K-leader rapidly accelerates again up to 20×10^6 m/s. The K-leader then decelerates to 10×10^6 m/s as it approaches the second junction at the flash origin (J2/O) around $320 \mu\text{s}$. After passing J2 the K-leader accelerates to 15×10^6 m/s at $385 \mu\text{s}$, before decelerating to 6×10^6 m/s as it approaches the third junction (J3) at $410 \mu\text{s}$. The K-leader then rapidly reaches its maximum speed of 25×10^6 m/s at $430 \mu\text{s}$, before gradually decelerating to 2×10^6 m/s at $1300 \mu\text{s}$. Variations occur within the gradual deceleration, but investigations into the nature of these variations will be left to future research.

235

236

237

238

239

240

The pattern observed is that when the K-leader approaches a branch junction it decelerates, and after it passes a junction it accelerates. Similar behavior has been observed for many other K-leaders in this flash, figures for these K-leaders are included in the supplementary material (Jensen et al., 2023). These common propagation behaviors are an interesting observation and can be explained as the following (Figure 6). We assume the K-leader speed is approximately proportional to the electric field strength at

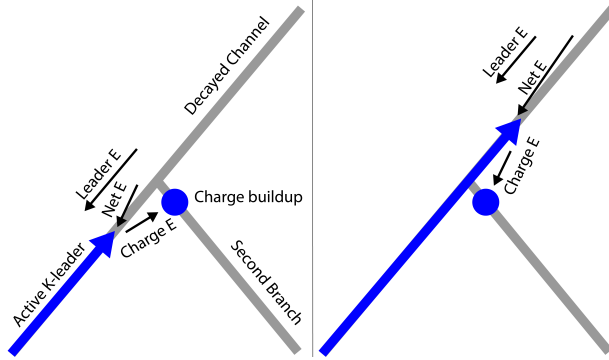


Figure 6. A simple diagram showing the hypothesized interaction of a K-leader with a charge deposit near a branch junction. “Leader E” is the electric field vector due to the negative K-leader, “Charge E” is the electric field vector due to the negative charge buildup near the junction, and “Net E” is the net electric field vector at the K-leader tip as the sum of the leader and charge field vectors. The length of each vector indicates the magnitude. As the K-leader approaches the junction the fields from the leader tip and deposited charge destructively interfere ($|Net \vec{E}| < |Leader \vec{E}|$). As the K-leader passes the junction the fields change to constructively interfere ($|Net \vec{E}| > |Leader \vec{E}|$). We assume K-leader speed is approximately proportional to the tip electric field magnitude. This diagram shows the simple case where there is no conductive connection between the branches.

241 the leader tip. When the branches are inactive prior to the K-leader, the channels are
 242 apparently poorly conductive. For different branches that have been active (conductive)
 243 alternately at different times, significant potential differences could be built between the
 244 branches, and this potential difference will lead to a charge deposit near the branch junc-
 245 tion. If the deposited charge is negative, when the active K-leader approaches the junc-
 246 tion the electric field at the leader tip will be decreased by the deposited charge, and this
 247 will slow down the active K-leader. Once the K-leader passes the junction the deposited
 248 charge along the inactive channel will on the other hand increase the field at the leader
 249 tip, leading to re-acceleration of the K-leader. It is also possible that the active K-leader
 250 increases the conductivity of the inactive branch while passing the junction. In this case,
 251 the conductive connection at the junction may further enhance the field at the passing
 252 K-leader tip and help to speed up the propagation even more. If the charge deposit at
 253 the branch junction is instead positive we would expect the opposite effect (acceleration
 254 followed by deceleration). If there is no significant charge deposit the junction is expected
 255 to have no effect on the speed. Between Figure 5 and the supplementary figures (Jensen
 256 et al., 2023) we have labeled 21 branch junction crossing where the leader speed during
 257 the crossing is well defined. Of these, only 2 cases appear to show little to no effect, the
 258 other 19 match the negative junction charge pattern.

259 This interpretation of the deceleration when a K-leader approaches a junction is
 260 further supported by K1, K3, and K5, which all stop at the first junction they meet. K1
 261 and K3 can be seen in Animation 2 and their corresponding figures in the supplemen-
 262 tary material (Jensen et al., 2023). As reported previously in 2D interferometer obser-
 263 vations (Shao & Krehbiel, 1996) and more recently in 3D observations (Shao et al., 2023),
 264 shorter K-leaders often stopped at a branch junction, indicating that sufficient negative
 265 charge was deposited near or at the junction points to reduce the electric field below the
 266 breakdown threshold at the leader tip.

267 In addition to the branch junction effect, other minor speed variations are observed
 268 throughout the K-leader development. We cannot point to a single factor that may cause
 269 these variations. We leave analysis of these variations to future investigations.

270 5 K-leader Electric Field Change

271 Two fast antennas are deployed with the BIMAP-3D system, one at each station.
 272 The two fast antennas have different effective gains due to the deployment setup. A rel-
 273 ative calibration was achieved between the two fast antennas by comparing the magni-
 274 tude of field changes for distant flashes (around 50 km from each station). Based on this
 275 comparison the fast antenna at BIMAP2 is more sensitive than that at BIMAP1 by a
 276 factor of 2, with an estimated uncertainty of 10%.

277 The amplifiers in the fast antennas also had different time constants (0.2 ms and
 278 1 ms), and the recorded field changes were “de-drooped” accordingly (Sonnenfeld et al.,
 279 2006; Födisch et al., 2016). The field change for each K-leader was de-drooped separately
 280 and the average field for a time period of 100 μ s before each K-leader was set to zero.
 281 The fast antenna signals were lowpassed at 50 kHz to focus on the electrostatic field com-
 282 ponent.

283 Using the recorded field changes from both stations, we modeled the electric field
 284 as being produced by a point charge at the leader tip. An opposite point charge was placed
 285 at the origin of the K-leader for charge conservation. This charge arrangement is a greatly
 286 simplified approximation of the charge distribution expected for an equipotential K-leader
 287 channel (Kasemir, 1960; Mazur & Ruhnke, 1998). The ground is assumed to behave like
 288 an infinite conducting plane. Then for a sensor located at a point (X, Y, Z) , where Z is
 289 the ground altitude at the station, the vertical electric field due to the two point charges
 290 at a given time is given by

$$E = \frac{-Q}{2\pi\epsilon_0} \left(\frac{z_1 - Z}{(x_1 - X)^2 + (y_1 - Y)^2 + (z_1 - Z)^2} - \frac{z_0 - Z}{(x_0 - X)^2 + (y_0 - Y)^2 + (z_0 - Z)^2} \right) \quad (1)$$

291 where (x_1, y_1, z_1) stands for the K-leader tip, (x_0, y_0, z_0) stands for the K-leader
 292 origin, and Q is the charge at the two points.

293 The magnitude of the charge Q in Equation 1 at a given time was estimated using
 294 a weighted least-squares fit between the two recorded field changes, accounting for
 295 the speed-of-light time delay between the leader tip and the respective fast antennas. The
 296 weighting was based on the total change of the field for the entire K-leader recorded by
 297 each fast antenna to avoid over-fitting to the closer antenna.

298 Figure 7 shows the modeled field at each station compared to the measured field
 299 (panels a and b) for K5, along with the variation in the modeled charge over time (panel
 300 c). The velocity and power over time are also included in the bottom panel (d) for com-
 301 parison. As shown in Figure 7, the point charge model is a good first order fit to the mea-
 302 sured field changes at both stations for K5. The modeled charge increases initially and
 303 then stays relatively constant for the rest of the K-leader duration. It is also observed
 304 that the increase in charge is generally correlated with the initial propagation acceler-
 305 ation and VHF power increase at the beginning of the K-leader.

306 It is important to note that this level of fit was only achieved for two of the K-leaders
 307 from this flash. Figure 7 shows the fit for K5, which propagated along a single branch
 308 (Figure 3). Similar results were observed for K1 (Figure 2), which travels along the same
 309 branch. K3 also developed along a single branch and showed similar charge behavior,
 310 but the quality of the fit to the measured fields changes was worse. This is possibly be-

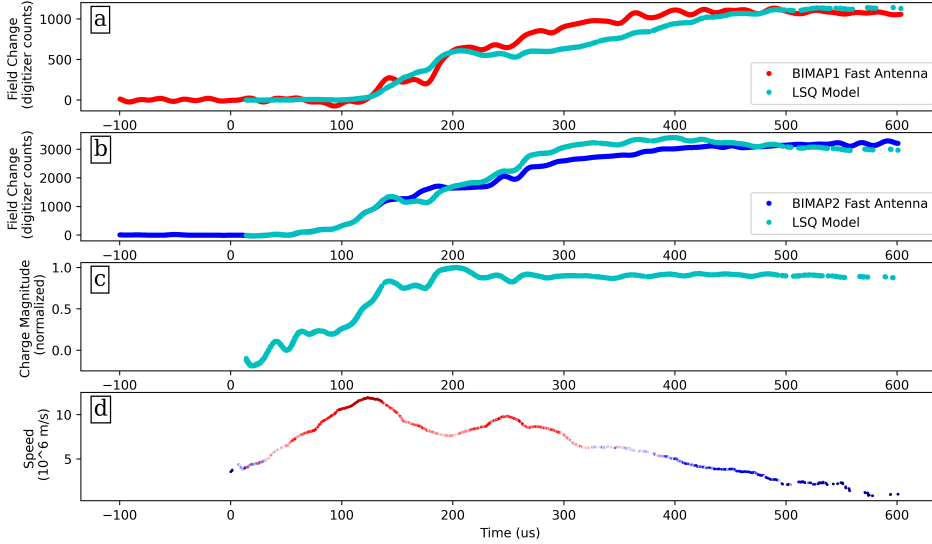


Figure 7. Plot of electric field change for K5 at BIMAP1 vs time (a), showing both the measured field change (red) and modeled field change (turquoise). Electric field change at BIMAP2 vs time (b), showing both the measured field change (blue) and modeled field change (turquoise). Modeled charge magnitude vs time (c), and speed vs time (d), colored by power.

311 cause the field change for K3 was small, and thus more dominated by local noise. The
 312 other K-leaders all pass multiple branch junctions (Figure 5, and supplementary figures
 313 (Jensen et al., 2023)), and cannot be fit with the simple two point charge model. In these
 314 cases the K-leader may redistribute charge along multiple branches as it passes a junc-
 315 tion. Even in the single branch case our two point model may be too simplified to ac-
 316 curately capture the evolution of the charge distribution on the channel, but this is one
 317 of the first attempts to explore this behavior.

318 6 VHF Sources Between K-leaders

319 Figure 8 shows the activity that occurs in the positive discharge region after the
 320 return stroke. Figure 8a is a Northing vs. Easting plot of the three main branches, which
 321 have been grouped into three separate data sets so that they can be analyzed individ-
 322 ually. The region containing these branches is marked out with a dashed border in Fig-
 323 ure 1b. The region in Figure 8 has been chosen to include essentially all sources in the
 324 positive breakdown region, while excluding the K-leaders themselves as much as possi-
 325 ble. The full development of this region, along with the K-leaders initiating from it, can
 326 be seen in Animation 2 in the supplementary material (Jensen et al., 2023).

327 Figures 8b, c, and d show the distance from the sources to the flash origin vs time
 328 for the west (red), center (green), and east (blue) branches respectively. The time at which
 329 a K-leader is launched on a particular branch is marked with a gray vertical line. In most
 330 cases K-leader sources are shown as a nearly vertical cluster that coincides with the gray
 331 vertical markers. In some cases, the K-leader initiates just outside of the analyzed re-
 332 gion and thus the sources do not appear in Figure 8.

333 Figure 8 shows three interesting insights into K-leader initiation and development.
 334 First, in every case the launch of a K-leader (at the times of the gray lines) is followed
 335 by an RF quiet period (typically 1-2 ms but sometimes exceeding 10 ms). The VHF sup-
 336 pression occurs specifically on the branch that launched the K-leader. Other branches

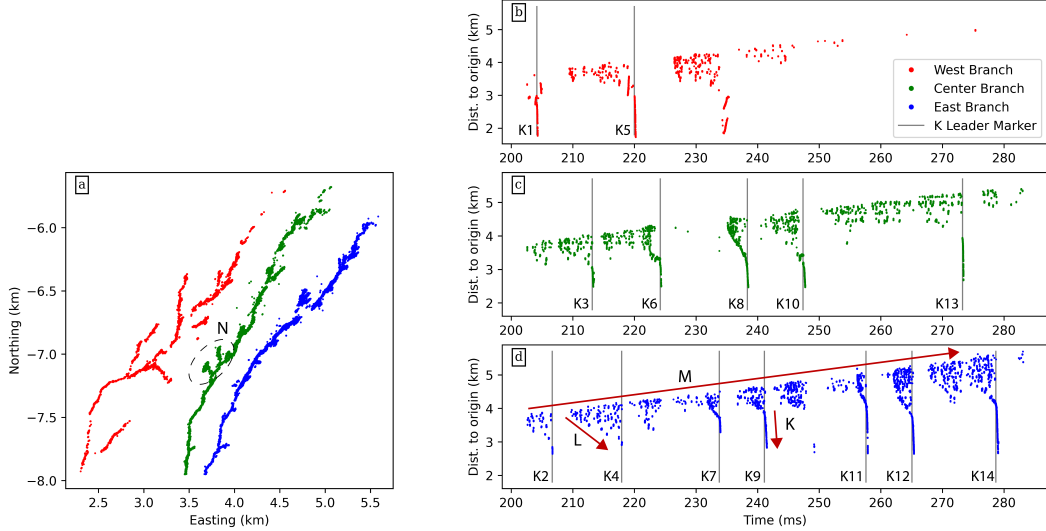


Figure 8. Northing vs. Easting plot of three manually separated branches of the positive leader (a), with plots of the distance from the flash origin vs. time for the west (b, red), center (c, green), and east (d, blue) branches. Gray vertical lines on the distance vs. time plots indicate that a K-leader began on that branch at that time. The K-leaders are labeled K1 through K14 chronologically.

337 may continue to emit VHF, or may also be suppressed. For example, the VHF suppression
 338 on the center channel (green, Figure 8c) after K3 does not occur on the other two
 339 branches (blue and red). On the other hand, K6 on the center branch (green, panel c)
 340 does seem to also suppress the east branch (blue, panel d). Hare et al. (2021) reported
 341 similar VHF suppression and referred to it as the K-leader “quenched” the activity on
 342 the channel.

343 Secondly, there appear to be three different types of processes that proceed at three
 344 different characteristic speeds. Examples of the three processes are labeled with arrows
 345 as K, L, and M in Figure 8d. The best understood, and fastest, of these are the K-leaders
 346 themselves, labeled K, typically initiating at speeds on the order of 10^6 m/s. The inter-
 347 mediate speed process, labeled L, is suggested by the downward slope at the bottom of
 348 each group of sources, and seems to extend at speeds on the order of 10^5 m/s. The slow-
 349 est process is the gentle upward source extension, labeled M, at speeds on the order of
 350 10^4 m/s. These three processes will be discussed further in Section 7.3.

351 Finally, it appears that the possible launch of a K-leader along one branch is some-
 352 times stopped by the initiation of a K-leader on a different branch. For instance the fea-
 353 tures of the scattered sources after K9 (between 243 ms and 248 ms) along the blue branch
 354 (Figure 8d) suggest a K-leader could soon be initiated, but instead K10 along the green
 355 branch occurs at this time. K10 apparently suppresses the scattered sources on both branches
 356 and appears to stop a K-leader from initiating on the blue branch. Similarly, K6 (green)
 357 appears to stop a K-leader on the blue branch. K11 and K12 (blue) also appear to stop
 358 K-leaders on the green branch. These observations indicate that neighboring branches
 359 can affect each other through the K-leader process.

7 Discussion

7.1 On Needles and “Twinkling”

We note that there are some small side-branches on the channels in Figure 8a, two examples on the center channel have been circled and labeled N. These small branches are the recently identified needles (Hare et al., 2019; 2021; Pu & Cummer, 2019). Saba et al. (2020) showed high speed video evidence of needles forming as failed branching attempts on upward positive leaders. Saba et al.’s suggested mechanism for needle formation is especially convincing because it explains why needles are typically inclined in the forward direction of the positive leader. In this study essentially all the protrusions from the channels are at 45° or less with the main channel (Figures 8a, 9a, and 9c). This is opposite to the orientation that would be expected if needles were formed originally by the negative end of a cut-off channel as proposed by Hare et al. (2019). The corona-field-reversal mechanism proposed by Pu and Cummer (2019) suggests that needles should be mostly orthogonal to the channel or uniformly distributed around 90° , which is also not consistent with our observations.

Regarding the VHF “flickering”, Stock et al. (2014) reported that positive leaders flickered in a somewhat random way, and Hare et al. (2019) reported that most of these flickering, or “twinkling”, sources are associated with needles. While the claim in Hare et al. (2019) appears to be true for the flash they analyzed, it is not clear that it is true in general. Hare et al. (2019) (their Figure 2) still shows a few twinkling sources that occur along the main channel but not clearly on needles, and the same is true for Hare et al. (2021) (their Figures 20 and 21). Pu and Cummer (2019) also showed many twinkling sources that are arguably on the main positive channel rather than on any needle (their Figure 2).

Our results in this study are shown in Figure 9, for two time intervals (top and bottom) between K-leaders. The left-hand panels (a and c) show the channel structure and location of the twinkling sources in northing vs. easting, where the background channel structure consists of all VHF sources in that region throughout the flash. The right-hand panels (b and d) show the twinkling sources in northing vs. time. In the bottom half of Figure 9a the twinkling sources seem to appear preferentially on the needles. The rest of the twinkling sources in Figures 9a and c seem to appear equally on needles and the main channel. The occurrence frequency of twinkles in Figures 9b and d also appears to be the same between sources on needles and on the channel.

We cannot rule out the presence of needles smaller than our spatial resolution, but in some areas in Figures 9a, and c twinkling sources seem to densely fill the channel. This does not seem consistent with sources occurring on distinct needle branches. Since their appearance in space and time is essentially the same, we consider all of the sources in Figures 8 and 9 to be VHF twinkling, except those associated with K-leaders. Other than appearing more commonly along the main channel our VHF twinkling observations are broadly in agreement with previous reports (Hare et al., 2019;2021; Pu & Cummer, 2019), although the individual twinkling events are too short in space and time for us to resolve their development.

Regarding the needle structures, our observations of needle orientation relative to the main channel, and high speed video observations of needle formation (Saba et al., 2020), indicate that ionized structures are already present prior to the detection of VHF-visible needles, and the needles sources simply occur on the pre-existing structures. The pre-ionized needle structures are apparently due to failed branching attempts of the VHF quiet positive leader tip. The observations of Hare et al. (2021) that subsequent twinkles on the same needle in general do not extend the needle length is consistent with our interpretation. Based on our observations VHF twinkling is associated with both the nee-

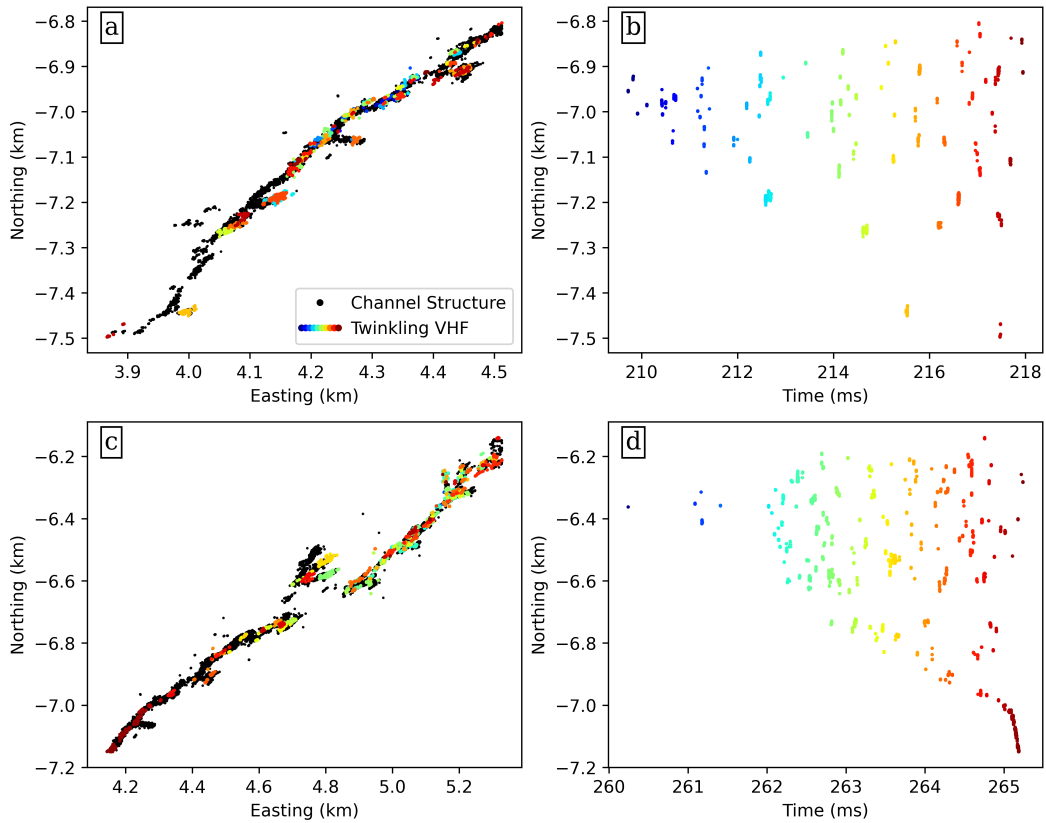


Figure 9. Two examples of twinkling behavior between K-leaders. The top panels show the location of twinkling sources and the background channel structure in Northing vs. Easting (a) and twinkling in Northing vs. time (b) for the period between K2 and K4, while the bottom panels show Northing vs. Easting (c), and Northing vs. time (d) for the period between K11 and K12. Both selections are on the east branch of Figure 8. The twinkling sources are colored by time.

410 dles (failed positive branches) and the main body of the positive channel, which are both
 411 part of the pre-ionized channel structure.

412 As an interesting observation, Figure 9b indicates that the twinkling rate is higher
 413 closer to the positive tip (further north in this case), and the distance between twinkling
 414 sources also seems to be smaller towards the tip. The fact that the same behaviors are
 415 more clear in Figure 9b than Figure 9d may be due to the fact that the majority of the
 416 twinkling sources appear within just 2.5 ms in Figure 9d, vs 10 ms in Figure 9b. Pu and
 417 Cummer (2019) also reported that the spatial and temporal density of twinkles was high-
 418 est near the forward tip.

419 As shown earlier in Figure 8, the downward slope of the southern edge of the twin-
 420 kling region, and the gentle average upward slope of the northern edge, are both appar-
 421 ent in Figure 9 panels b and d. Our interpretation of these upward and downward slopes
 422 will be discussed in Section 7.3.

423 7.2 Quenching vs Masking

424 With LMA observations of a triggered upward positive leader, Edens et al. (2012)
 425 reported that temporal gaps in the positive leader sources seemed to correspond to si-
 426 multaneous lower altitude negative breakdown. They attributed this to the masking of
 427 higher power negative sources over the weaker positive sources. Although this masking
 428 could play a role in suppressing VHF sources on the positive leader, K3 in this study (green,
 429 Figure 8c) does not interrupt the twinkling on the other two branches (red and blue).
 430 There are multiple examples in this flash where a K-leader occurs with simultaneous on-
 431 going VHF twinkling on the other branches. For instance, this occurs for K1 and K5 on
 432 the red branch, K8 and K13 on the green branch, and K9 on the blue branch.

433 We can thus infer that the quenching of VHF sources is a real effect, presumably
 434 caused by a change in the physical state of the channel during and after a K-leader. The
 435 fact that after quenching the twinkling sources re-start near the apparent positive tip
 436 before extending back towards the origin also points to a physical change in the chan-
 437 nel conditions.

438 High speed video observations show K-leaders significantly increasing the channel
 439 luminosity (Kong et al., 2008; Saba et al., 2008; Warner et al., 2012; Mazur, 2016; Wang
 440 et al., 2019; Huang et al., 2021; Jiang et al., 2022; Ding et al., 2022), indicating increased
 441 temperature and conductivity along the channel at that time. Since this is coincident
 442 with the suppression of VHF twinkling in this study, we can infer that the increased con-
 443 ductivity is the reason for the VHF quenching. In the cases where a K-leader quenches
 444 multiple channels, there must be a conductive connection between those branches. For
 445 instance, after K10 on the green branch (Figure 8c) the twinkling along the blue branch
 446 (panel d) is also suppressed. Such an inter-connection is consistent with our discussion
 447 of K-leaders displacing charge along multiple branches in Section 5, and with our sug-
 448 gession that a K-leader can interrupt the initiation of other K-leaders (Section 6).

449 The duration of VHF quenching should therefore be related to the decay time for
 450 a conductive K-leader channel to become non-conductive. Shao et al. (2012) predicted
 451 that the decay time for a dart leader channel can be approximated as $\tau = 0.17e^{z/2.3}$ (ms),
 452 where z is altitude in km. At 6 km where the K-leaders started in this study, the decay
 453 time would be 2.3 ms. This is surprisingly close to the typical quenching duration ob-
 454 served in Figure 8.

455 If quenching is caused by the increased conductivity of the K-leader channel, the
 456 masking observed by Edens et al. (2012) may have been caused by the same effect. Their
 457 observations are generally consistent with the upward positive leader branches produc-
 458 ing downward K-leaders, and in some cases these K-leaders may have quenched all the

459 positive leader branches. On the other hand the LMA is probably more susceptible to
 460 masking because of its longer integration windows compared to BIMAP-3D (10 μ s-100 μ s
 461 compared to ~ 0.5 μ s).

462 7.3 Three Characteristic Speeds in the Positive Breakdown Region

463 Among the three characteristic speeds in Figure 8, the fastest is the K-leader it-
 464 self starting on the order of 10^6 m/s (labeled K), which consists of negative breakdown
 465 and is clearly visualized by BIMAP-3D. The slowest process on the order of 10^4 m/s (la-
 466 beled M) is associated with the extension of the positive leaders. Since we generally do
 467 not see the positive leader tip itself in VHF (Pu et al., 2021; Stock et al., 2023) it is not
 468 surprising that this extension seems to continue whether VHF is observed or not. This
 469 is most obvious in Figure 8b where very few VHF sources were detected after 250 ms
 470 but the upward slope is still apparent. Even though the observed VHF sources are prob-
 471 ably not at the positive leader tips, it is reasonable to assume that the true positive leader
 472 tip is at a roughly fixed distance ahead. In Figure 8, the average extension speed of all
 473 three branches is the same, 2×10^4 m/s. It is interesting to note that the occurrence
 474 of K-leaders does not appear to have any significant effect on this extension speed.

475 The intermediate speed process on the order of 10^5 m/s (Figure 8d, labeled L) is
 476 difficult to interpret. A more detailed view of this development is shown in Figures 9b
 477 and d. This speed is associated with the extension of the VHF twinkling region towards
 478 the direction of the flash origin, but not related to any well defined channel propagation.
 479 Although this extension leads to the start of the next K-leader, with our current obser-
 480 vations we do not understand the physical mechanism for this process. Nevertheless this
 481 process is clearly associated with K-leader initiation because the downward development
 482 in Figures 8c and d generally continues until either a K-leader is initiated or the process
 483 is interrupted by a K-leader from another channel.

484 Optical observations by other researchers show that the channel is dark before a
 485 K-leader initiates (Kong et al., 2008; Mazur, 2016; Wang et al., 2019; Huang et al., 2021;
 486 Jiang et al., 2022; Ding et al., 2022). In Section 7.2 we argued that VHF twinkling was
 487 suppressed on a conductive channel. Taking these together it suggest that the process
 488 that causes VHF twinkling and that initiates K-leaders should occur on relatively cold/low
 489 conductivity channels.

490 Hare et al. (2021) and Pu and Cummer (2019) both reported on the forward ex-
 491 tension of the twinkling region along a channel with similar distance vs time plots to our
 492 Figure 8 (their Figures 22 and 4 respectively). Pu and Cummer (2019) estimated a 2D
 493 average speed of 1×10^5 m/s for this forward progression, Hare et al. (2021) reports $5 \times$
 494 10^4 m/s for their case, both are higher than our estimated speed of 2×10^4 m/s. In ad-
 495 dition, they did not observe the intermediate speed process progressing towards the di-
 496 rection of the flash origin, nor did they report any K-leaders during this interval. In our
 497 study the progression towards the flash origin seems to be a feature of twinkling specifi-
 498 cally at the stage when K-leaders are being actively produced.

499 All the VHF twinkling in Figures 8 and 9 is probably the same process we iden-
 500 tified as “blooming” in Jensen et al. (2021). The spatial and temporal resolution in Jensen
 501 et al. (2021) was insufficient to identify the extension forward and expansion back to-
 502 ward the flash origin, or to make the association with reported observations of VHF twin-
 503 kling on needles.

504 7.4 Slow Positive Leaders May Generally be Dim

505 Figures 8 and 9 show scattered VHF twinkling sources in the positive discharge re-
 506 gion, and in Section 7.3 we argued that this takes place on a dark channel. Similar VHF
 507 twinkling on the positive leader is observed in the early part of the flash, starting 20 ms

508 into the flash (Figure 1a, around 8 km). The similarity in the source scattering and slow
 509 extension ($\sim 10^4$ m/s) between these two stages of the flash suggests that the positive
 510 leader may also be dim in the early part of the flash. Bright positive leaders have been
 511 observed in high speed video in other studies, but the reported leader speed is typically
 512 one to two orders of magnitude higher (10^5 m/s- 10^6 m/s) (Saba et al., 2008; Campos
 513 et al., 2014; Kong et al., 2015), suggesting the reported optical positive leaders develop
 514 under different circumstances as compared to the slow in-cloud development as presented
 515 in this paper. Some studies have reported optical observations with evidence of dim or
 516 dark positive leaders extending on the order of 10^4 m/s (Kong et al., 2008; Wang et al.,
 517 2019; Jiang et al., 2022).

518 7.5 The Life Cycle of a K-leader

519 Based on the observations presented in this paper, the life-cycle in the simplest case
 520 is as follows: Following a period of VHF twinkling, a K-leader is initiated. The K-leader
 521 then accelerates with increasing charge at both tips, and then the K-leader gradually de-
 522 celerates to a stop with a relatively constant charge at the tips. After a few milliseconds
 523 of VHF quiet period, the twinkling process starts again, and that will lead to the ini-
 524 tiation of the next K-leader. We have already discussed the processes leading to the ini-
 525 tiation of a K-leader in Section 7.3. We now discuss the physical mechanisms that drive
 526 the rest of the K-leader development.

527 Let us first attempt to explain the initial acceleration of the K-leader. The speed
 528 of the K-leader should primarily depend on the electric field strength at the negative leader
 529 tip, and the state of conditioning of the channel to be retraced by the K-leader. Since
 530 the K-leader channel becomes hot once it is started, as observed optically (Kong et al.,
 531 2008; Saba et al., 2008; Warner et al., 2012; Mazur, 2016; Ding et al., 2022), the active
 532 leader section can be treated as conductive and approximately equipotential. For an equipo-
 533 tential channel in a uniform electric field the field strength as well as the charge concen-
 534 tration at the tip would increase linearly with channel length (Kasemir, 1960; Mazur &
 535 Ruhnke, 1998). In this case it is not difficult to understand the leader acceleration as
 536 it propagates forward.

537 However, at the late lightning stage during the K-leader phase the electric field around
 538 the lightning structures cannot be assumed uniform. Earlier discharges prior to the K-
 539 leaders have redistributed charge along the channel structures, and the electric field at
 540 any position would be a superposition of the general background field and the disturbed
 541 field due to the lightning itself. Nevertheless, at the far extremes of the positive break-
 542 down region where the K-leaders are initiated, the local field is likely dominated by the
 543 nearby negative charge concentration in the cloud and is less affected by the main light-
 544 ning structure. In a small spatial scale in this region, the field can be assumed uniform
 545 and directed toward the negative charge in the cloud. Under such considerations, the ac-
 546 celeration along a short section of the leader propagation can be understood.

547 On the other hand, as the K-leader propagates away from the negative cloud charge
 548 region and toward the main channel structure the lightning-induced charge redistribu-
 549 tion acts as an increasingly more dominant factor. Since previous discharge processes
 550 effectively transported negative charge toward the region near and beyond the origin of
 551 the flash, the field strength at the active leader tip will be continuously reduced as it prop-
 552 agates toward this region. Under these conditions, the K-leader is expected to slow down
 553 after its initial acceleration. This also explains why most K-leaders stop at the origin of
 554 the flash and sometimes at branch junctions, especially for simple IC flashes (e.g., Shao
 555 and Krehbiel, 1996; Shao et al., 2023). The other factor that helps to slow down the leader
 556 propagation is the energy dissipation due to the re-ionization of the pre-established but
 557 cold channel, as discussed in Jensen et al. (2021). However, based on the common de-

558 velopment behavior of the K-leaders it appears that the local field plays a dominant role
 559 on its initial acceleration and later deceleration.

560 8 Summary

561 The results in this paper can be briefly summarized as follows:

- 562 1. K-leader propagation speed generally exhibits an initial acceleration followed by
 563 a gradual deceleration, though the development of individual K-leaders is often
 564 complex.
- 565 2. K-leader VHF power is exponentially correlated with speed.
- 566 3. K-leaders often enter a step-like propagation mode at around 1×10^6 m/s in their
 567 final stages, and peak VHF power in this step-like mode can be comparable to the
 568 VHF power emitted by K-leaders at their maximum speed.
- 569 4. Branch junctions affect K-leader speed, and may affect charge redistribution.
- 570 5. In simple cases the K-change can be modeled as time-evolving equal and oppo-
 571 site charges at the K-leader origin and propagating negative tip.
- 572 6. The estimated charge magnitude at the K-leader tip increases initially, then stays
 573 relatively constant.
- 574 7. The initial acceleration and charge buildup of K-leaders can be explained by the
 575 equipotential model.
- 576 8. The gradual deceleration of K-leaders may be due to charge deposited along the
 577 channel by earlier lightning processes.
- 578 9. VHF twinkling is not unique to needles, it also occurs on the main channel.
- 579 10. We have confirmed that K-leaders quench VHF twinkling, and the quenching is
 580 a real physical effect, not an observational artifact.
- 581 11. After quenching, the VHF twinkling region extends forward in the positive break-
 582 down direction at $\sim 10^4$ m/s, and back towards the origin at $\sim 10^5$ m/s.
- 583 12. K-leaders are initiated by the extending twinkling process on an optically dark/low
 584 conductivity channel.
- 585 13. A K-leader from one branch may interrupt progress towards initiation of a K-leader
 586 on other branches.
- 587 14. Slow positive leaders ($\sim 10^4$ m/s) may generally be optically dark while they ex-
 588 hibit VHF twinkling.

589 Appendix A Speed Uncertainty Analysis

We can relate the speed uncertainty to the position uncertainty by expressing the speed (V) as the difference in time and location of two points

$$V = \sqrt{\left(\frac{x_1 - x_2}{t_1 - t_2}\right)^2 + \left(\frac{y_1 - y_2}{t_1 - t_2}\right)^2 + \left(\frac{z_1 - z_2}{t_1 - t_2}\right)^2} \quad (\text{A1})$$

The uncertainty, expressed as a standard deviation will be of the form

$$\sigma_V = \sum_i \sum_j \left(\frac{\partial V}{\partial i}\right) \left(\frac{\partial V}{\partial j}\right) \sigma_i \sigma_j \quad (\text{A2})$$

590 where the sums for i and j are over each variable, $x_1, x_2, y_1, y_2, z_1, z_2, t_1$, and t_2 .

The partial derivatives of V can be summarized as

$$\frac{\partial V}{\partial x_1} = \frac{1}{V} \frac{x_1 - x_2}{(t_1 - t_2)^2} = \frac{V_x}{V \Delta t} \quad (\text{A3})$$

$$\frac{\partial V}{\partial x_2} = -\frac{1}{V} \frac{x_1 - x_2}{(t_1 - t_2)^2} = -\frac{V_x}{V \Delta t} \quad (\text{A4})$$

$$\frac{\partial V}{\partial t_1} = -\frac{1}{V} \frac{(x_1 - x_2)^2 + (y_1 - y_2)^2 + (z_1 - z_2)^2}{(t_1 - t_2)^3} = -\frac{V}{\Delta t} \quad (\text{A5})$$

$$\frac{\partial V}{\partial t_2} = \frac{1}{V} \frac{(x_1 - x_2)^2 + (y_1 - y_2)^2 + (z_1 - z_2)^2}{(t_1 - t_2)^3} = \frac{V}{\Delta t} \quad (\text{A6})$$

591 where $\Delta t = t_1 - t_2$, $V_x = \frac{x_1 - x_2}{\Delta t^2}$, and the equations are symmetric for x , y , and z .

592 Computing Equation A2 from the partial derivatives, and assuming the uncertain-
593 ties are the same for both points (i.e. $\sigma_{x_1} = \sigma_{x_2}$, etc.), we can see that most of the terms
594 will cancel out since half of the partial derivatives are negative and half are positive. Thus
595 we are left with only the squared terms

$$\sigma_V^2 = \left[\left(\frac{V_x}{V \Delta t} \right)^2 \sigma_x^2 + \left(\frac{V_y}{V \Delta t} \right)^2 \sigma_y^2 + \left(\frac{V_z}{V \Delta t} \right)^2 \sigma_z^2 + \left(\frac{V}{\Delta t} \right)^2 \sigma_t^2 \right] \quad (\text{A7})$$

If we make a conservative error estimate so that we can assume $\sigma_x = \sigma_y = \sigma_z = c \sigma_t$, where c is the speed of light, then we can combine terms to get

$$\sigma_V^2 = \sigma_x^2 \left[\frac{1}{\Delta t^2} + \frac{V^2}{c^2 \Delta t^2} \right] \quad (\text{A8})$$

Recognizing that $\frac{V^2}{c^2} \ll 1$ for any reasonable lightning activity we can drop the second term (associated with σ_t) and are left with

$$\sigma_V = \frac{\sigma_x}{|\Delta t|} \quad (\text{A9})$$

596 If we further assume that we have N points and are taking an average of all of the
597 possible finite differences ($\frac{1}{2}N(N-1)$ combinations) rather than a single finite differ-
598 ence then we can apply the central limit theorem and get

$$\sigma_{\overline{V}} = \sqrt{\frac{2}{N(N-1)}} \frac{\sigma_x}{|\overline{\Delta t}|} \quad (\text{A10})$$

599 where $\sigma_{\overline{V}}$ is the standard deviation of the average speed, and $\overline{\Delta t}$ is the average time
600 difference between points.

601 While this averaging method is not identical to the linear fit method used for re-
602 sults presented in Figures 2-5, it is tractable to an analytic solution. The linear fit method
603 was also evaluated via a Monte Carlo simulation.

604 Parameters for the uncertainty estimation and the resulting uncertainties were de-
605 termined as follows: Shao et al. (2023) showed that in an ideal case the random loca-
606 tion uncertainty of BIMAP-3D can be better than 10 m in all directions (x , y , and z).
607 For the purpose of estimating the speed uncertainty we will use a more conservative es-
608 timate of 30 m location uncertainty in all directions for the K-leaders analyzed. If we
609 further assume that in a typical 30 μs window we have about 30 sources (an underes-
610 timate), and the average time difference between sources is about 1/4 the window size,
611 then from Equation A10 we get an estimated speed uncertainty of 2×10^5 m/s. A Monte

612 Carlo simulation was also conducted by repeatedly adding random offsets in each direc-
 613 tion (Easting, Northing, and altitude) to each source location and then recalculating the
 614 speeds as compared to the non-offset values. For offsets that were normally distributed
 615 with a standard deviation of 30 m this method also yielded a one sigma uncertainty of
 616 2×10^5 m/s.

617 Larger speed uncertainties can be caused when sources are coming from multiple
 618 branches at the same time, especially when the branches are close to each other so they
 619 are hard to separate in the data, but these errors are typically obvious as brief extreme
 620 fluctuations in the measured speed and can be excluded from the analysis.

621 Appendix B Open Research

622 All data used for this paper are placed at <https://doi.org/10.5281/zenodo.8213032>
 623 (Jensen et al., 2023), along with some supplementary animations and figures. All data
 624 files are in text format with headers that describe each data column. A PDF is included
 625 which describes the included files, and gives examples of the headers and column format.

626 Acknowledgments

627 Research presented in this article was supported by the Laboratory Directed Re-
 628 search and Development program of Los Alamos National Laboratory under project num-
 629 ber 20230223ER.

630 References

- 631 Akita, M., Nakamura, Y., Yoshida, S., Morimoto, T., Ushio, T., Kawasaki, Z., &
 632 Wang, D. (2010). What occurs in k process of cloud flashes? *Journal of*
 633 *Geophysical Research: Atmospheres*, 115(D7). Retrieved from [https://](https://agupubs.onlinelibrary.wiley.com/doi/abs/10.1029/2009JD012016)
 634 agupubs.onlinelibrary.wiley.com/doi/abs/10.1029/2009JD012016 doi:
 635 10.1029/2009JD012016
- 636 Campos, L. Z., Saba, M. M., Warner, T. A., Pinto, O., Krider, E. P., & Orville,
 637 R. E. (2014). High-speed video observations of natural cloud-to-ground light-
 638 ning leaders – a statistical analysis. *Atmospheric Research*, 135-136, 285-305.
 639 Retrieved from [https://www.sciencedirect.com/science/article/pii/](https://www.sciencedirect.com/science/article/pii/S0169809513000057)
 640 [S0169809513000057](https://www.sciencedirect.com/science/article/pii/S0169809513000057) doi: <https://doi.org/10.1016/j.atmosres.2012.12.011>
- 641 Ding, Z., Rakov, V. A., Zhu, Y., Kereszy, I., Chen, S., & Tran, M. D. (2022). A
 642 positive leader intermittently extending via bidirectional transients and pro-
 643 ducing a negative cloud-to-ground lightning flash. *AGU Fall Meeting 2022*.
 644 Retrieved from [https://agu2022fallmeeting-agu.ipostersessions.com/](https://agu2022fallmeeting-agu.ipostersessions.com/Default.aspx?s=BC-DB-C9-DA-C0-85-DD-28-4F-E0-9E-65-07-76-EB-D0(AE35A-0064))
 645 [Default.aspx?s=BC-DB-C9-DA-C0-85-DD-28-4F-E0-9E-65-07-76-EB-D0](https://agu2022fallmeeting-agu.ipostersessions.com/Default.aspx?s=BC-DB-C9-DA-C0-85-DD-28-4F-E0-9E-65-07-76-EB-D0(AE35A-0064))
 646 (AE35A-0064)
- 647 Edens, H. E., Eack, K. B., Eastvedt, E. M., Trueblood, J. J., Winn, W. P., Krehbiel,
 648 P. R., ... Thomas, R. J. (2012). Vhf lightning mapping observations of a
 649 triggered lightning flash. *Geophysical Research Letters*, 39(19). Retrieved
 650 from [https://agupubs.onlinelibrary.wiley.com/doi/abs/10.1029/](https://agupubs.onlinelibrary.wiley.com/doi/abs/10.1029/2012GL053666)
 651 [2012GL053666](https://agupubs.onlinelibrary.wiley.com/doi/abs/10.1029/2012GL053666) doi: <https://doi.org/10.1029/2012GL053666>
- 652 Födisch, P., Wohsmann, J., Lange, B., Schönherr, J., Enghardt, W., & Kaever, P.
 653 (2016). Digital high-pass filter deconvolution by means of an infinite impulse
 654 response filter. *Nuclear Instruments and Methods in Physics Research Section*
 655 *A: Accelerators, Spectrometers, Detectors and Associated Equipment*, 830, 484-
 656 496. Retrieved from [https://www.sciencedirect.com/science/article/](https://www.sciencedirect.com/science/article/pii/S0168900216305617)
 657 [pii/S0168900216305617](https://www.sciencedirect.com/science/article/pii/S0168900216305617) doi: <https://doi.org/10.1016/j.nima.2016.06.019>
- 658 Hare, B. M., Scholten, O., Buitink, S., Dwyer, J. R., Liu, N., Sterpka, C., & ter
 659 Veen, S. (2023, Jan). Characteristics of recoil leaders as observed by lofar.

- 660 *Phys. Rev. D*, 107, 023025. Retrieved from [https://link.aps.org/doi/](https://link.aps.org/doi/10.1103/PhysRevD.107.023025)
 661 10.1103/PhysRevD.107.023025 doi: 10.1103/PhysRevD.107.023025
- 662 Hare, B. M., Scholten, O., Dwyer, J., Strepka, C., Buitink, S., Corstanje, A., ...
 663 Winchen, T. (2021). Needle propagation and twinkling characteristics. *Journal*
 664 *of Geophysical Research: Atmospheres*, 126(6), e2020JD034252. Retrieved
 665 from [https://agupubs.onlinelibrary.wiley.com/doi/abs/10.1029/](https://agupubs.onlinelibrary.wiley.com/doi/abs/10.1029/2020JD034252)
 666 2020JD034252 (e2020JD034252 2020JD034252) doi: [https://doi.org/10.1029/](https://doi.org/10.1029/2020JD034252)
 667 2020JD034252
- 668 Hare, B. M., Scholten, O., Dwyer, J., Trinh, T., Buitink, S., Ter Veen, S., ... oth-
 669 ers (2019). Needle-like structures discovered on positively charged light-
 670 ning branches. *Nature*, 568(7752), 360–363. doi: [https://doi.org/10.1038/](https://doi.org/10.1038/s41586-019-1086-6)
 671 s41586-019-1086-6
- 672 Huang, H., Wang, D., Wu, T., & Takagi, N. (2021). Recoil leader and associated
 673 discharge features observed during the progression of a multi-branched up-
 674 ward lightning flash. *Journal of Geophysical Research: Atmospheres*, 126(24),
 675 e2021JD035162. Retrieved from [https://agupubs.onlinelibrary.wiley](https://agupubs.onlinelibrary.wiley.com/doi/abs/10.1029/2021JD035162)
 676 [.com/doi/abs/10.1029/2021JD035162](https://doi.org/10.1029/2021JD035162) (e2021JD035162 2021JD035162) doi:
 677 <https://doi.org/10.1029/2021JD035162>
- 678 Jensen, D. P., Shao, X.-M., & Sonnenfeld, R. (2023, August). *Data and Sup-*
 679 *plementary Material for “Insights into Lightning K-Leader Initiation and*
 680 *Development from Three Dimensional Broadband Interferometric Observa-*
 681 *tions” by Jensen et al.* Zenodo. Retrieved from [https://doi.org/10.5281/](https://doi.org/10.5281/zenodo.8213032)
 682 zenodo.8213032 ([Dataset]) doi: 10.5281/zenodo.8213032
- 683 Jensen, D. P., Sonnenfeld, R. G., Stanley, M. A., Edens, H. E., da Silva, C. L., &
 684 Krehbiel, P. R. (2021). Dart-leader and k-leader velocity from initiation
 685 site to termination time-resolved with 3d interferometry. *Journal of Geo-*
 686 *physical Research: Atmospheres*, e2020JD034309. Retrieved from [https://](https://agupubs.onlinelibrary.wiley.com/doi/abs/10.1029/2020JD034309)
 687 [agupubs.onlinelibrary.wiley.com/doi/abs/10.1029/2020JD034309](https://doi.org/10.1029/2020JD034309) doi:
 688 <https://doi.org/10.1029/2020JD034309>
- 689 Jiang, R., Yuan, S., Qie, X., Liu, M., & Wang, D. (2022). Activation of abun-
 690 dant recoil leaders and their promotion effect on the negative-end break-
 691 down in an intracloud lightning flash. *Geophysical Research Letters*, 49(1),
 692 e2021GL096846. Retrieved from [https://agupubs.onlinelibrary.wiley](https://agupubs.onlinelibrary.wiley.com/doi/abs/10.1029/2021GL096846)
 693 [.com/doi/abs/10.1029/2021GL096846](https://doi.org/10.1029/2021GL096846) (e2021GL096846 2021GL096846) doi:
 694 <https://doi.org/10.1029/2021GL096846>
- 695 Jordan, D. M., Idone, V. P., Rakov, V. A., Uman, M. A., Beasley, W. H., & Ju-
 696 renka, H. (1992). Observed dart leader speed in natural and triggered light-
 697 ning. *Journal of Geophysical Research: Atmospheres*, 97(D9), 9951-9957.
 698 Retrieved from [https://agupubs.onlinelibrary.wiley.com/doi/abs/](https://agupubs.onlinelibrary.wiley.com/doi/abs/10.1029/92JD00566)
 699 10.1029/92JD00566 doi: 10.1029/92JD00566
- 700 Kasemir, H. W. (1960). A contribution to the electrostatic theory of a lightning
 701 discharge. *Journal of Geophysical Research (1896-1977)*, 65(7), 1873-1878.
 702 Retrieved from [https://agupubs.onlinelibrary.wiley.com/doi/abs/](https://agupubs.onlinelibrary.wiley.com/doi/abs/10.1029/JZ065i007p01873)
 703 10.1029/JZ065i007p01873 doi: <https://doi.org/10.1029/JZ065i007p01873>
- 704 Kitagawa, N. (1957). On the mechanism of cloud flash and junction or final process
 705 in flash to ground. *Papers in Meteorology and Geophysics*, 7(4), 415-424. doi:
 706 10.2467/mripapers1950.7.4_415
- 707 Kong, X., Qie, X., & Zhao, Y. (2008). Characteristics of downward leader in a
 708 positive cloud-to-ground lightning flash observed by high-speed video camera
 709 and electric field changes. *Geophysical Research Letters*, 35(5). Retrieved
 710 from [https://agupubs.onlinelibrary.wiley.com/doi/abs/10.1029/](https://agupubs.onlinelibrary.wiley.com/doi/abs/10.1029/2007GL032764)
 711 2007GL032764 doi: <https://doi.org/10.1029/2007GL032764>
- 712 Kong, X., Zhao, Y., Zhang, T., & Wang, H. (2015). Optical and electrical char-
 713 acteristics of in-cloud discharge activity and downward leaders in positive
 714 cloud-to-ground lightning flashes. *Atmospheric Research*, 160, 28-38. Re-

- 715 trieved from [https://www.sciencedirect.com/science/article/pii/](https://www.sciencedirect.com/science/article/pii/S0169809515000721)
716 S0169809515000721 doi: <https://doi.org/10.1016/j.atmosres.2015.02.014>
- 717 Loeb, L. B. (1966). The mechanisms of stepped and dart leaders in cloud-to-ground
718 lightning strokes. *Journal of Geophysical Research (1896-1977)*, 71(20), 4711-
719 4721. Retrieved from [https://agupubs.onlinelibrary.wiley.com/doi/abs/](https://agupubs.onlinelibrary.wiley.com/doi/abs/10.1029/JZ071i020p04711)
720 10.1029/JZ071i020p04711 doi: 10.1029/JZ071i020p04711
- 721 Mazur, V. (2002). Physical processes during development of lightning flashes.
722 *Comptes Rendus Physique*, 3(10), 1393-1409. Retrieved from [https://](https://www.sciencedirect.com/science/article/pii/S1631070502014123)
723 www.sciencedirect.com/science/article/pii/S1631070502014123 doi:
724 [https://doi.org/10.1016/S1631-0705\(02\)01412-3](https://doi.org/10.1016/S1631-0705(02)01412-3)
- 725 Mazur, V. (2016). The physical concept of recoil leader formation. *Journal of*
726 *Electrostatics*, 82, 79–87. Retrieved from [https://www.sciencedirect.com/](https://www.sciencedirect.com/science/article/pii/S0304388616300407)
727 [science/article/pii/S0304388616300407](https://www.sciencedirect.com/science/article/pii/S0304388616300407) doi: [https://doi.org/10.1016/](https://doi.org/10.1016/j.elstat.2016.05.005)
728 [j.elstat.2016.05.005](https://doi.org/10.1016/j.elstat.2016.05.005)
- 729 Mazur, V., & Ruhnke, L. H. (1998). Model of electric charges in thunderstorms and
730 associated lightning. *Journal of Geophysical Research: Atmospheres*, 103(D18),
731 23299-23308. Retrieved from [https://agupubs.onlinelibrary.wiley.com/](https://agupubs.onlinelibrary.wiley.com/doi/abs/10.1029/98JD02120)
732 [doi/abs/10.1029/98JD02120](https://agupubs.onlinelibrary.wiley.com/doi/abs/10.1029/98JD02120) doi: <https://doi.org/10.1029/98JD02120>
- 733 Pu, Y., & Cummer, S. A. (2019). Needles and lightning leader dynam-
734 ics imaged with 100–200 mhz broadband vhf interferometry. *Geophys-*
735 *ical Research Letters*, 46(22), 13556-13563. Retrieved from [https://](https://agupubs.onlinelibrary.wiley.com/doi/abs/10.1029/2019GL085635)
736 agupubs.onlinelibrary.wiley.com/doi/abs/10.1029/2019GL085635 doi:
737 <https://doi.org/10.1029/2019GL085635>
- 738 Pu, Y., Cummer, S. A., & Liu, N. (2021). Vhf radio spectrum of a positive leader
739 and implications for electric fields. *Geophysical Research Letters*, 48(11),
740 e2021GL093145. Retrieved from [https://agupubs.onlinelibrary.wiley](https://agupubs.onlinelibrary.wiley.com/doi/abs/10.1029/2021GL093145)
741 [.com/doi/abs/10.1029/2021GL093145](https://agupubs.onlinelibrary.wiley.com/doi/abs/10.1029/2021GL093145) (e2021GL093145 2021GL093145) doi:
742 <https://doi.org/10.1029/2021GL093145>
- 743 Rakov, V. A., & Uman, M. A. (2003). *Lightning: physics and effects*. Cambridge
744 university press.
- 745 Saba, M. M. F., Cummins, K. L., Warner, T. A., Krider, E. P., Campos, L. Z. S.,
746 Ballarotti, M. G., ... Fleenor, S. A. (2008). Positive leader characteristics
747 from high-speed video observations. *Geophysical Research Letters*, 35(7).
748 Retrieved from [https://agupubs.onlinelibrary.wiley.com/doi/abs/](https://agupubs.onlinelibrary.wiley.com/doi/abs/10.1029/2007GL033000)
749 10.1029/2007GL033000 doi: <https://doi.org/10.1029/2007GL033000>
- 750 Saba, M. M. F., de Paiva, A. R., Concollato, L. C., Warner, T. A., & Schumann, C.
751 (2020). Optical observation of needles in upward lightning flashes. *Scientific*
752 *Reports*, 10(1), 17460. doi: <https://doi.org/10.1038/s41598-020-74597-6>
- 753 Saraiva, A. C. V., Campos, L. Z. S., Williams, E. R., Zepka, G. S., Alves, J.,
754 Pinto Jr., O., ... Blakeslee, R. J. (2014). High-speed video and electro-
755 magnetic analysis of two natural bipolar cloud-to-ground lightning flashes.
756 *Journal of Geophysical Research: Atmospheres*, 119(10), 6105-6127. Retrieved
757 from [https://agupubs.onlinelibrary.wiley.com/doi/abs/10.1002/](https://agupubs.onlinelibrary.wiley.com/doi/abs/10.1002/2013JD020974)
758 2013JD020974 doi: <https://doi.org/10.1002/2013JD020974>
- 759 Schonland, B. F. J., Malan, D. J., Collens, H., & Boys, C. V. (1935). Progres-
760 sive lightning ii. *Proceedings of the Royal Society of London. Series A -*
761 *Mathematical and Physical Sciences*, 152(877), 595-625. Retrieved from
762 <https://royalsocietypublishing.org/doi/abs/10.1098/rspa.1935.0210>
763 doi: 10.1098/rspa.1935.0210
- 764 Shao, X.-M., Ho, C., Bowers, G., Blaine, W., & Dingus, B. (2020). Lightning
765 interferometry uncertainty, beam steering interferometry, and evidence of
766 lightning being ignited by a cosmic ray shower. *Journal of Geophysical Re-*
767 *search: Atmospheres*, 125(19), e2019JD032273. Retrieved from [https://](https://agupubs.onlinelibrary.wiley.com/doi/abs/10.1029/2019JD032273)
768 agupubs.onlinelibrary.wiley.com/doi/abs/10.1029/2019JD032273
769 (e2019JD032273 2019JD032273) doi: <https://doi.org/10.1029/2019JD032273>

- 770 Shao, X.-M., Ho, C., Caffrey, M., Graham, P., Haynes, B., Bowers, G., ...
 771 Rassoul, H. (2018). Broadband rf interferometric mapping and po-
 772 larization (bimap) observations of lightning discharges: Revealing new
 773 physics insights into breakdown processes. *Journal of Geophysical Re-*
 774 *search: Atmospheres*, 123(18), 10,326-10,340. Retrieved from [https://](https://agupubs.onlinelibrary.wiley.com/doi/abs/10.1029/2018JD029096)
 775 agupubs.onlinelibrary.wiley.com/doi/abs/10.1029/2018JD029096 doi:
 776 <https://doi.org/10.1029/2018JD029096>
- 777 Shao, X.-M., Jensen, D., Ho, C., Graham, P., Haynes, W., Caffrey, M., ... Sonnen-
 778 feld, R. (2023). Three-dimensional broadband interferometric mapping and
 779 polarization (bimap-3d) observations of lightning discharge processes. *Journal*
 780 *of Geophysical Research: Atmospheres*, e2022JD037955.
- 781 Shao, X. M., & Krehbiel, P. R. (1996). The spatial and temporal development of in-
 782 tracloud lightning. *Journal of Geophysical Research: Atmospheres*, 101(D21),
 783 26641-26668. Retrieved from [https://agupubs.onlinelibrary.wiley.com/](https://agupubs.onlinelibrary.wiley.com/doi/abs/10.1029/96JD01803)
 784 [doi/abs/10.1029/96JD01803](https://agupubs.onlinelibrary.wiley.com/doi/abs/10.1029/96JD01803) doi: 10.1029/96JD01803
- 785 Shao, X. M., Krehbiel, P. R., Thomas, R. J., & Rison, W. (1995). Radio interfero-
 786 metric observations of cloud-to-ground lightning phenomena in florida. *Journal*
 787 *of Geophysical Research: Atmospheres*, 100(D2), 2749-2783. Retrieved from
 788 <https://agupubs.onlinelibrary.wiley.com/doi/abs/10.1029/94JD01943>
 789 doi: 10.1029/94JD01943
- 790 Shao, X.-M., Lay, E., & Jacobson, A. R. (2012). On the behavior of return stroke
 791 current and the remotely detected electric field change waveform. *Journal*
 792 *of Geophysical Research: Atmospheres*, 117(D7). Retrieved from [https://](https://agupubs.onlinelibrary.wiley.com/doi/abs/10.1029/2011JD017210)
 793 agupubs.onlinelibrary.wiley.com/doi/abs/10.1029/2011JD017210 doi:
 794 <https://doi.org/10.1029/2011JD017210>
- 795 Shao, X. M., Rhodes, C. T., & Holden, D. N. (1999). Rf radiation obser-
 796 vations of positive cloud-to-ground flashes. *Journal of Geophysical Re-*
 797 *search: Atmospheres*, 104(D8), 9601-9608. Retrieved from [https://](https://agupubs.onlinelibrary.wiley.com/doi/abs/10.1029/1999JD900036)
 798 agupubs.onlinelibrary.wiley.com/doi/abs/10.1029/1999JD900036 doi:
 799 <https://doi.org/10.1029/1999JD900036>
- 800 Sonnenfeld, R. G., Battles, J. D., Lu, G., & Winn, W. P. (2006). Compar-
 801 ing e field changes aloft to lightning mapping data. *Journal of Geo-*
 802 *physical Research: Atmospheres*, 111(D20). Retrieved from [https://](https://agupubs.onlinelibrary.wiley.com/doi/abs/10.1029/2006JD007242)
 803 agupubs.onlinelibrary.wiley.com/doi/abs/10.1029/2006JD007242 doi:
 804 <https://doi.org/10.1029/2006JD007242>
- 805 Stock, M. G., Akita, M., Krehbiel, P. R., Rison, W., Edens, H. E., Kawasaki, Z.,
 806 & Stanley, M. A. (2014). Continuous broadband digital interferometry of
 807 lightning using a generalized cross-correlation algorithm. *Journal of Geophys-*
 808 *ical Research: Atmospheres*, 119(6), 3134-3165. Retrieved from [https://](https://agupubs.onlinelibrary.wiley.com/doi/abs/10.1002/2013JD020217)
 809 agupubs.onlinelibrary.wiley.com/doi/abs/10.1002/2013JD020217 doi:
 810 <https://doi.org/10.1002/2013JD020217>
- 811 Stock, M. G., Tilles, J., Taylor, G. B., Dowell, J., & Liu, N. (2023). Lightning in-
 812 terferometry with the long wavelength array. *Remote Sensing*, 15(14). Re-
 813 trieved from <https://www.mdpi.com/2072-4292/15/14/3657> doi: 10.3390/
 814 rs15143657
- 815 Stolzenburg, M., Marshall, T. C., Karunarathne, S., Karunarathna, N., & Orville,
 816 R. E. (2015). Transient luminosity along negative stepped leaders in light-
 817 ning. *Journal of Geophysical Research: Atmospheres*, 120(8), 3408-3435.
 818 Retrieved from [https://agupubs.onlinelibrary.wiley.com/doi/abs/](https://agupubs.onlinelibrary.wiley.com/doi/abs/10.1002/2014JD022933)
 819 [10.1002/2014JD022933](https://agupubs.onlinelibrary.wiley.com/doi/abs/10.1002/2014JD022933) doi: <https://doi.org/10.1002/2014JD022933>
- 820 Wang, X., Zhao, X., Cai, H., Liu, G., Liao, M., & Qu, L. (2019). Optical charac-
 821 teristics of branched downward positive leader associated with recoil leader
 822 activity. *Journal of Atmospheric and Solar-Terrestrial Physics*, 196, 105158.
 823 Retrieved from [https://www.sciencedirect.com/science/article/pii/](https://www.sciencedirect.com/science/article/pii/S1364682619304274)
 824 [S1364682619304274](https://www.sciencedirect.com/science/article/pii/S1364682619304274) doi: <https://doi.org/10.1016/j.jastp.2019.105158>

- 825 Warner, T. A., Cummins, K. L., & Orville, R. E. (2012). Upward lightning ob-
826 servations from towers in rapid city, south dakota and comparison with
827 national lightning detection network data, 2004–2010. *Journal of Geo-*
828 *physical Research: Atmospheres*, 117(D19). Retrieved from [https://](https://agupubs.onlinelibrary.wiley.com/doi/abs/10.1029/2012JD018346)
829 agupubs.onlinelibrary.wiley.com/doi/abs/10.1029/2012JD018346 doi:
830 <https://doi.org/10.1029/2012JD018346>
- 831 Winn, W. P., Aulich, G. D., Hunyady, S. J., Eack, K. B., Edens, H. E., Kre-
832 hbiel, P. R., ... Sonnenfeld, R. G. (2011). Lightning leader stepping, k
833 changes, and other observations near an intracloud flash. *Journal of Geo-*
834 *physical Research: Atmospheres*, 116(D23). Retrieved from [https://](https://agupubs.onlinelibrary.wiley.com/doi/abs/10.1029/2011JD015998)
835 agupubs.onlinelibrary.wiley.com/doi/abs/10.1029/2011JD015998 doi:
836 [10.1029/2011JD015998](https://doi.org/10.1029/2011JD015998)
- 837 Zhu, B., Zhou, H., Thottappillil, R., & Rakov, V. A. (2014). Simultaneous ob-
838 servations of electric field changes, wideband magnetic field pulses, and vhf
839 emissions associated with k processes in lightning discharges. *Journal of Geo-*
840 *physical Research: Atmospheres*, 119(6), 2699-2710. Retrieved from [https://](https://agupubs.onlinelibrary.wiley.com/doi/abs/10.1002/2013JD021006)
841 agupubs.onlinelibrary.wiley.com/doi/abs/10.1002/2013JD021006 doi:
842 <https://doi.org/10.1002/2013JD021006>